Analytica Chimica Acta 851 (2014) 95–102

Contents lists available at ScienceDirect

Analytica Chimica Acta

journal homepage: www.elsevier.com/locate/aca

Synergistic electrocatalytic effect of nanostructured mixed films formed by functionalised gold nanoparticles and bisphthalocyanines

C. Medina-Plaza [a], L.N. Furini [a,b], C.J.L. Constantino [b], J.A. de Saja [c], M.L. Rodriguez-Mendez [a,*]

[a] Universidad de Valladolid, Department of Inorganic Chemistry, Engineers School, Spain
[b] Faculdade de Ciências e Tecnologia, UNESP Univ Estadual Paulista, 19060-900 Presidente Prudente, SP, Brazil
[c] Universidad de Valladolid, Department of Condensed Matter Physics, Faculty of Sciences, Spain

HIGHLIGHTS

- Gold nanoparticles and lutetium bisphthalocyanine have been co-deposited using the LB technique.
- Films used as voltammetric sensors provide enhanced responses towards hydroquinone.
- The efficient electrocatalytic properties are due to synergistic effects.

GRAPHICAL ABSTRACT

Sensors based on gold nanoparticles and lutetium bisphthalocyanine, co-deposited using Langmuir–Blodgett technique, have demonstrated improved sensing properties towards hydroquinone due to synergistic effects.

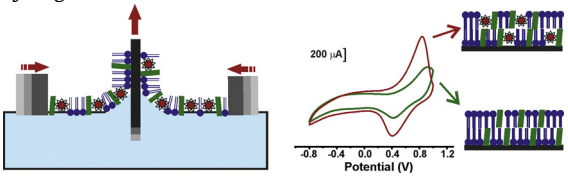

ARTICLE INFO

Article history:
Received 30 May 2014
Received in revised form 28 July 2014
Accepted 25 August 2014
Available online 2 September 2014

Keywords:
Gold nanoparticle
Bisphthalocyanine
Langmuir–Blodgett
Sensor
Hydroquinone

ABSTRACT

A synergistic electrocatalytic effect was observed in sensors where two electrocatalytic materials (functionalized gold nanoparticles and lutetium bisphthalocyanine) were co-deposited using the Langmuir–Blodgett technique. Films were prepared using a novel method where water soluble functionalised gold nanoparticles [(11-mercaptoundecyl)tetra(ethylene glycol)] (SAuNPs) were inserted in floating films of lutetium bisphthalocyanine ($LuPc_2$) and dimethyldioctadecylammonium bromide (DODAB) as the amphiphilic matrix. The formation of stable and homogeneous mixed films was confirmed by π-A isotherms, BAM, UV–vis and Raman spectroscopy, as well as by SEM and TEM microscopy. The synergistic effect towards hydroquinone of the electrodes modified with $LuPc_2$:DODAB/SAuNP was characterised by an increase in the intensity of the redox peaks and a reduction of the overpotential. This synergistic electrocatalytic effect arose from the interaction between the SAuNPs and the phthalocyanines that occur in the Langmuir–Blodgett films and from the high surface area provided by the nanostructured films. The sensitivity increased with the amount of $LuPc_2$ and SAuNPs inserted in the films and limits of detection in the range of 10^{-7} mol L^{-1} were attained.

1. Introduction

Phenolic compounds are a large family of molecules which are widely distributed in plant-derived foods. They have attracted great interest due to their potential health benefits. Polyphenolic compounds also contribute to the organoleptic characteristics of foods and affect their antioxidant capacity [1]. The determination of phenols can be carried out using traditional techniques including spectroscopy, gas or liquid chromatography and electrochemical methods. Oxidation of phenols is feasible at inert electrodes (i.e. metallic or glassy carbon electrodes) [2] and at electrodes chemically modified with a variety of materials and biomaterials [3]. The modification of the electrode surface with nanomaterials has demonstrated to be a good strategy to prepare

* Corresponding author at: Department of Inorganic Chemistry, Escuela de Ingenierías Industriales, Paseo del Cauce, 59, 47011 Valladolid, Spain. Tel.: +34 983 423540; fax: +34 983 423310.
E-mail address: mluz@eii.uva.es (M.L. Rodriguez-Mendez).

http://dx.doi.org/10.1016/j.aca.2014.08.049
0003-2670/

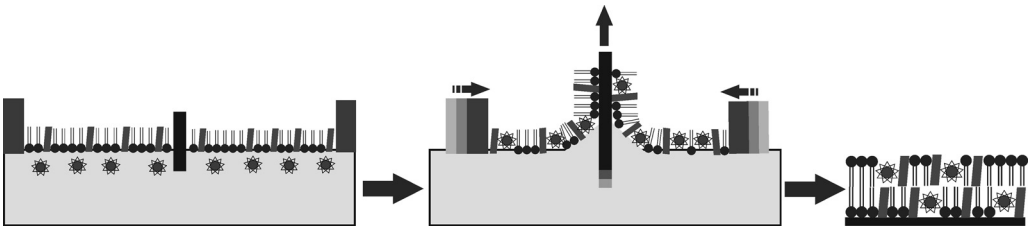

Fig. 1. Method to prepare the $LuPc_2$:DODAB/SAuNP films: DODAB, $LuPc_2$, SAuNP.

sensing devices [4,5]. For instance, electrodes modified with gold nanoparticles (AuNPs) show unique catalytic properties that depend on the AuNP size and on the nature of the protecting groups. In addition, AuNPs provide a large surface area for the detection of analytes, leading to electrochemical sensors with lower detection limits [6–9].

On the other hand, metallophthalocyanines (MPc) and their sandwich type lanthanide derivatives ($LnPc_2$) have demonstrated to behave as excellent sensing materials for the detection of a variety of compounds due to their well-known electrocatalytic properties, fast electron transfer and electron mediator capabilities [10–18].

The design of hybrid systems combining different electrocatalytic materials is very attractive for the development of electrochemical sensors. Recently, AuNPs and phthalocyanines have been successfully combined at a sensor surface using spin coating [19,20]. However, the applications of these composite AuNP/MPc systems require the development of methods allowing both classes of compounds to be co-immobilised in structures with controlled distribution of the two components [21,22].

The LB technique can be an alternative to produce nanostructured multilayers where two or more compounds are co-deposited in mixed films [23]. The materials used to form the films must fulfil the particular requirements of these techniques. For instance, in classical LB deposition, the film-forming materials must be amphiphilic molecules (insoluble in water but soluble in organic solvents). This means that the AuNPs must be capped (i.e. with thiolate groups) which facilitate the adequate dispersion onto the water subphase [24,25]. In turn, to obtain phthalocyanine multilayer assemblies, it is often necessary to mix the phthalocyanines with amphiphiles such as fatty acids or phospholipids that induce flexibility in the monolayers facilitating the transfer to solid substrates [15,18].

In this work, a new method was developed to co-deposit LB films of phthalocyanines with gold nanoparticles. The method consisted in the insertion of water soluble gold nanoparticles [(11-mercaptoundecyl)tetra(ethylene glycol)] (SAuNP) underneath a floating Langmuir film formed by a phthalocyanine [lutetium (III) bisphthalocyanine] and an amphiphile [dimethyldioctadecylammonium bromide] (DODAB). The insertion of the SAuNPs into the nanostructured $LuPc_2$:DODAB floating film to obtain $LuPc_2$:DODAB/SAuNP films was evaluated using spectroscopic and microscopic techniques. Then, the sensing capabilities of films containing different proportions of $LuPc_2$:DODAB and increasing amounts of SAuNP were studied using cyclic voltammetry. In the present work, we focus the attention on the determination of hydroquinone, an antioxidant belonging to the phenols family commonly found in foods such as teas or wines [26]. The synergistic effect caused by the interaction of two electrocatalytic materials: the SAuNPs and the $LuPc_2$ will be discussed.

2. Materials and methods

The lutetium (III) bisphthalocyaninate ($LuPc_2$) was synthesised and purified in the neutral radical state using a previously published method [27]. (11-Mercaptoundecyl)tetra(ethylene glycol) functionalised gold nanoparticles (SAuNP), dimethyldioctadecylammonium bromide (DODAB), and all the chemicals and solvents were purchased from Sigma–Aldrich and Fluka.

Buffer phosphate 0.01 M (pH 7.0) was prepared mixing sodium phosphate monobasic (purity >99%) and sodium phosphate dibasic (purity 99%) in ultrapure water.

LB films were prepared in a KSV 2000 System Langmuir–Blodgett trough equipped with a Wilhelmy plate to measure the surface pressure vs. mean molecular area (π-A) isotherms.

Films containing $LuPc_2$ and DODAB ($LuPc_2$:DODAB) were prepared by spreading a chloroform solution of the corresponding mixture (10:1), (1:1) or (1:10) (1×10^{-5} mol L^{-1}) onto a water subphase (ultrapure water–Millipore MilliQ kept at 20 °C). Then, the barriers were compressed at a speed of 10 mm min^{-1} to register the π-A isotherms. At a surface pressure of 35 mN m^{-1}, 20 monolayers were transferred to the solid substrates by Z type deposition with a transfer ratio close to 1.

Films containing SAuNP, DODAB and $LuPc_2$ ($LuPc_2$:DODAB/SAuNP), were prepared from chloroform mixtures $LuPc_2$:DODAB (10:1), (1:1) and (1:10) that were spread onto the water subphase. After evaporation of the solvent, 100 or 500 μL of an aqueous solution of SAuNP (0.02% w/v) were injected drop by drop underneath the air–water interface (before compressing the film) and adsorbed inside the floating monolayer. Floating layers of $LuPc_2$:DODAB/SAuNP were compressed and transferred to solid substrates using the same conditions mentioned in the previous paragraph. 20 monolayers LB films were built by Z type deposition with a transfer ratio close to 1. A scheme of the preparation method is shown in Fig. 1. The complete list of the sensors prepared is collected in Table 1.

Langmuir films were analysed with Brewster Angle Microscopy (BAM) using a KSV MicroBAM. UV–vis absorption measurements were conducted using a Shimadzu spectrophotometer UV-1603. TEM images were recorded using a JEM-FS2200 HRP instrument.

Raman analysis was performed in a Raman spectrometer UV-HR Lab Ram from Horiba–Jobin Ybon, equipped with a LN2-cooled charge-coupled device (CCD) detector. The excitation was carried out with different lasers, including an Nd–YAG laser (emitting at 532 nm) and a He–Ne laser (emitting at 633 nm), with a spectral resolution of 1 cm^{-1}. The sample was excited through the 50× optical objective of a Leica microscope. The scattered light was collected through the same optical objective (back-scattering configuration) with ca. 1 μm spatial resolution.

Table 1
List of the sensors prepared in this work.

Film	Proportion $LuPc_2$:DODAB	Vol. SAuNPs added (μL)
$LuPc_2$:DODAB (10:1)	10:01	0
$LuPc_2$:DODAB/SAuNP (10:1/100)	10:01	100
$LuPc_2$:DODAB/SAuNP (10:1/500)	10:01	500
$LuPc_2$:DODAB (1:1)	01:01	0
$LuPc_2$:DODAB/SAuNP (1:1/100)	01:01	100
$LuPc_2$:DODAB/SAuNP (1:1/500)	01:01	500
$LuPc_2$:DODAB (1:10)	01:10	0
$LuPc_2$:DODAB/SAuNP (1:10/100)	01:10	100
$LuPc_2$:DODAB/SAuNP (1:10/500)	01:10	500

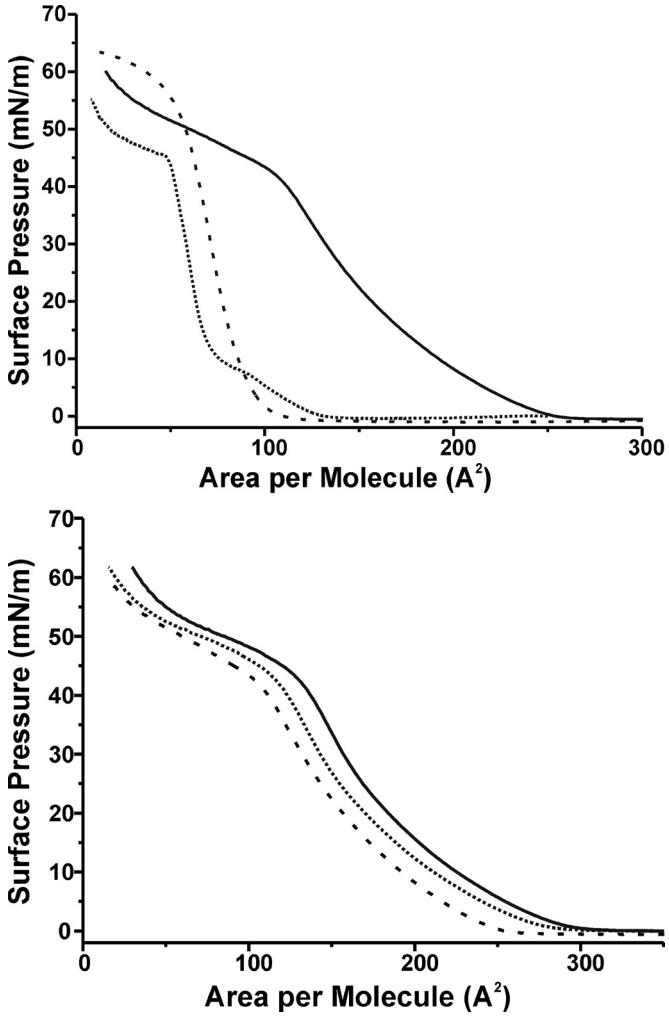

Fig. 2. Surface pressure/area per molecule isotherms. Top: $LuPc_2$:DODAB (10:1) (dashed line); $LuPc_2$:DODAB (1:1) (solid line) and $LuPc_2$:DODAB (1:10) (dotted line).

The excitation power on the sample surface was kept below 100 kW cm^{-2}.

The electrochemistry was carried out in an EG&G PARC 273 potentiostat/galvanostat using a conventional three-electrode cell. The LB films were used as working electrodes. The reference electrode was Ag|AgCl/KCl 3 M, and the counter electrode was a platinum plate.

3. Results and discussion

3.1. Langmuir monolayers

The π-A isotherms of mixtures of $LuPc_2$:DODAB (proportions 10:1 1:1 and 1:10) were registered by spreading the corresponding chloroform mixture onto the water subphase and compressing the barriers at a speed of 10 mm min^{-1} while registering the variations of the surface pressure (Fig. 2, top). When the proportion of $LuPc_2$ was high (10:1), the isotherms were compatible with a total miscibility of the two components. The calculated limiting area of 90 $Å^2$ was in agreement with the limiting area previously reported for $LuPc_2$ and corresponds to an edge-on orientation with the Pc ring perpendicular to the water subphase [28–30]. When DODAB was the majority component (1:10), the π-A isotherms showed a classical pattern of immiscibility consisting of two regions of different slope. At low pressures, the slope of the curve was 127 $Å^2$ coinciding with the limiting area registered for neat DODAB [31], whereas in the second steep rise of the surface pressure, the limiting area calculated was 90 $Å^2$ that coincided with the value of neat $LuPc_2$. The π-A isotherm of the equimolar mixture $LuPc_2$:DODAB (1:1), was consistent with a miscible system and showed a large area per molecule of 240 $Å^2$. This expansion of the monolayer could be due to repulsive interactions between $LuPc_2$ and DODAB or change of molecular accommodation at the surface [32].

SAuNPs were inserted in the $LuPc_2$:DODAB floating films by injecting the nanoparticles underneath the air–water interface. The insertion of the gold nanoparticles in the floating films was confirmed by the expansion of the area per molecule that increased with the amount of SAuNPs injected under the surface (Fig. 2, bottom). The expansion of the monolayer was clear in $LuPc_2$:DODAB mixtures 10:1 and 1:1. In contrast, in 1:10 films (low concentration of $LuPc_2$), the insertion of SAuNP was almost negligible suggesting that the insertion of the SAuNP was mainly due to the conjugation of SAuNPs to the phthalocyanine molecules. It is also important to indicate that injecting amounts of SAuNPs higher than 500 μL, caused irreproducibility, probably due to the occurrence of phase segregation.

The quality of the floating films was further analysed using Brewster Angle Microscopy (BAM). In the absence of SAuNP, Langmuir films showed highly homogeneous surfaces. Films containing SAuNP showed a granular structure as a result of the insertion of the nanoparticles in the floating film. This is illustrated in Fig. 3 where the BAM images of $LuPc_2$:DODAB and $LuPc_2$:DODAB/SAuNP films are compared.

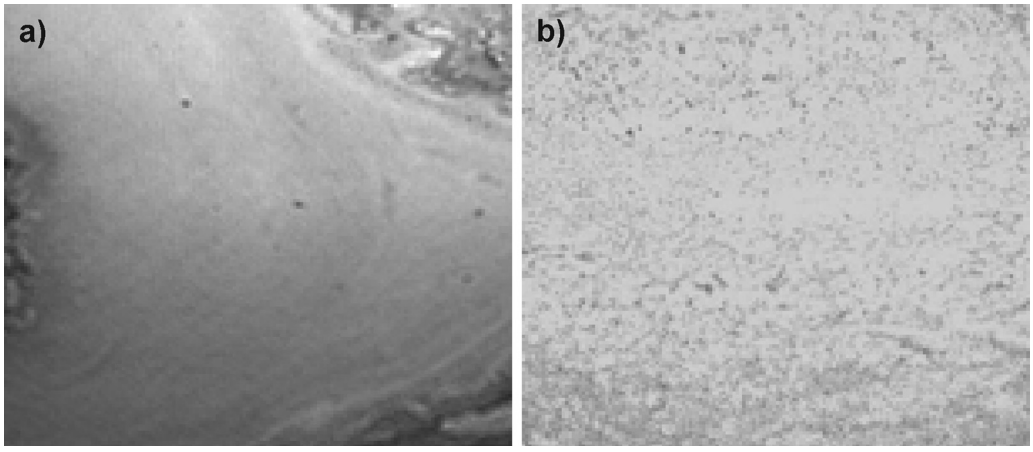

Fig. 3. BAM images of (a) LuPc2:DODAB (1:1) and (b) LuPc2:DODAB/SAuNP (1:1/100).

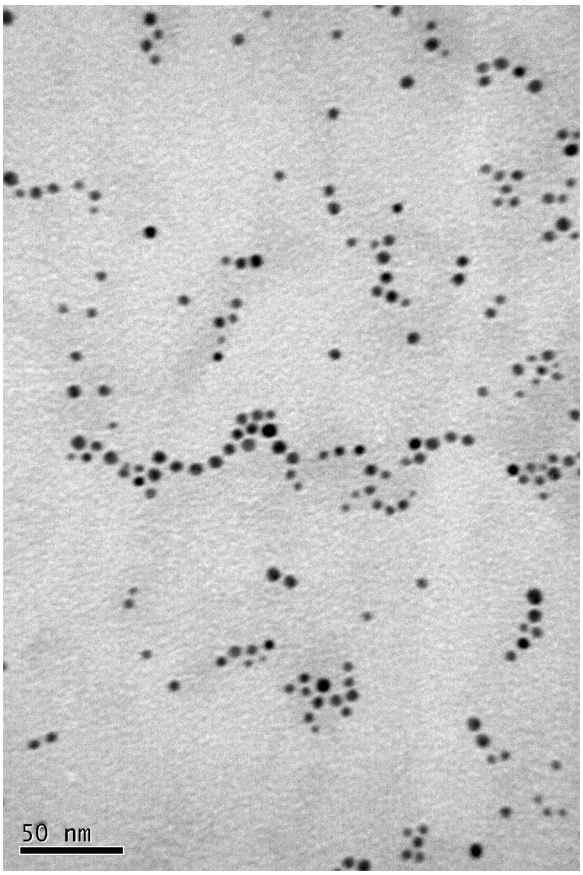

Fig. 4. TEM images of the LuPc2:DODAB/SAuNP (1:1/100).

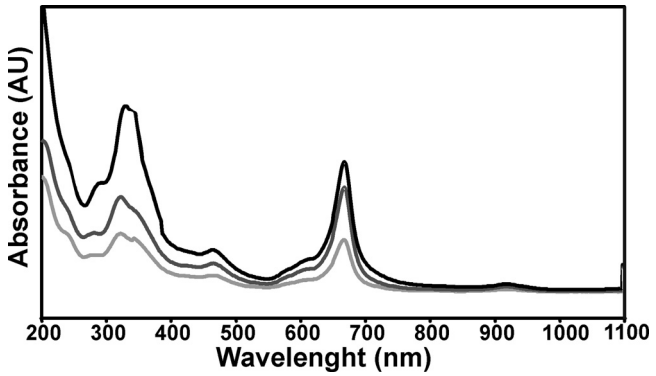

Fig. 5. UV–vis spectra of 20 monolayers LB films of LuPc2:DODAB (1:1) (light grey); LuPc2:DODAB/SAuNP (1:1/100) (dark grey) and LuPc2:DODAB/SAuNP (1:1/500) (black).

3.2. Langmuir–Blodgett films

3.2.1. Characterisation

The Langmuir films were transferred to solid substrates. The structure of the films deposited on a copper grid coated with carbon film was examined using TEM (Fig. 4). TEM images showed domains at micrometre scale formed by $LuPc_2$:DODAB. The gold cores of the nanoparticles were observed as bright spots of 3.5–5.0 nm that coincided well with the core diameter of the SAuNPs used in this work. The SAuNPs were homogeneously distributed on the surface and were preferentially distributed in the border between $LuPc_2$:DODAB domains.

The UV–vis absorption spectra of the $LuPc_2$:DODAB films deposited onto quartz substrates were characterised by a Q band at 665 nm and a Soret band at 340 nm produced by π–π^* transitions of the phthalocyanine ring (Fig. 5). These values were in good accordance with the results reported for $LuPc_2$ and arachidic acid mixtures [28].

The intensity of the bands increased with the proportion of $LuPc_2$ (1:10 > 1:1 > 10:1), in accordance with the Lambert–Beer's Law. The increase in the $LuPc_2$ proportion also caused a shift of the Q band to higher wavelengths (660 nm for the mixture 1:10; 665 nm for 1:1 and 675 nm for 10:1) indicating a higher level of aggregation and an extension of the aromaticity. The presence of J-aggregates in head-to-tail arrangement of transition dipoles in the LB film is responsible for this effect [33]. When inserting SAuNP particles in the structures, the Q and Soret bands increased their intensity. This enhancement was proportional to the amount of SAuNP introduced in the films, suggesting that the amplification was caused by the interaction between the phthalocyanine and the gold nanoparticles (the plasmon resonance of the SAuNP overlaps with the Q band of the $LuPc_2$ [34]). In addition, the magnification caused by the SAuNPs increased proportionally with the proportion of DODAB used. This fact could be explained taking into account that DODAB decreases the degree of aggregation of the tightly packed phthalocyanine molecules, facilitating the interaction between $LuPc_2$ and the SAuNP.

The LB films were investigated using micro-Raman technique, which combines morphological and chemical information at micrometre scale by coupling an optical microscope to a Raman spectrograph. Raman spectra recorded with the 633 nm line are illustrated in Fig. 6. Since the $LuPc_2$ absorbs the 633 nm laser line used here, the resonance Raman scattering (RRS) should take place [35].

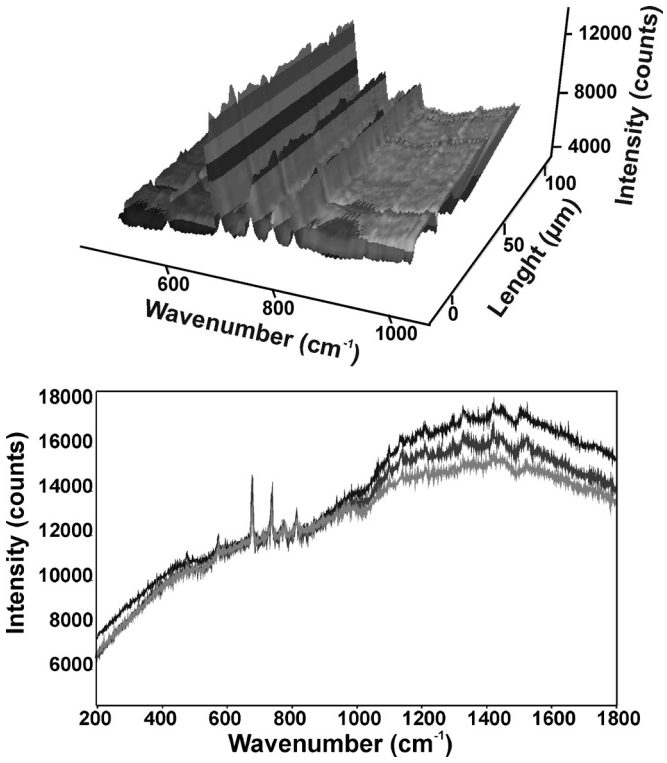

Fig. 6. Resonant Raman spectra registered using the 633 nm laser line: Top: 3D line Raman mapping for a 10 monolayers LB film of LuPc2:DODAB/SAuNP (1:1/100). Down: Raman spectra collected from LuPc2:DODAB (1:1) (light grey); LuPc2: DODAB/SAuNP (1:1/100) (dark grey) and LuPc2:DODAB/SAuNP (1:1/500) (black).

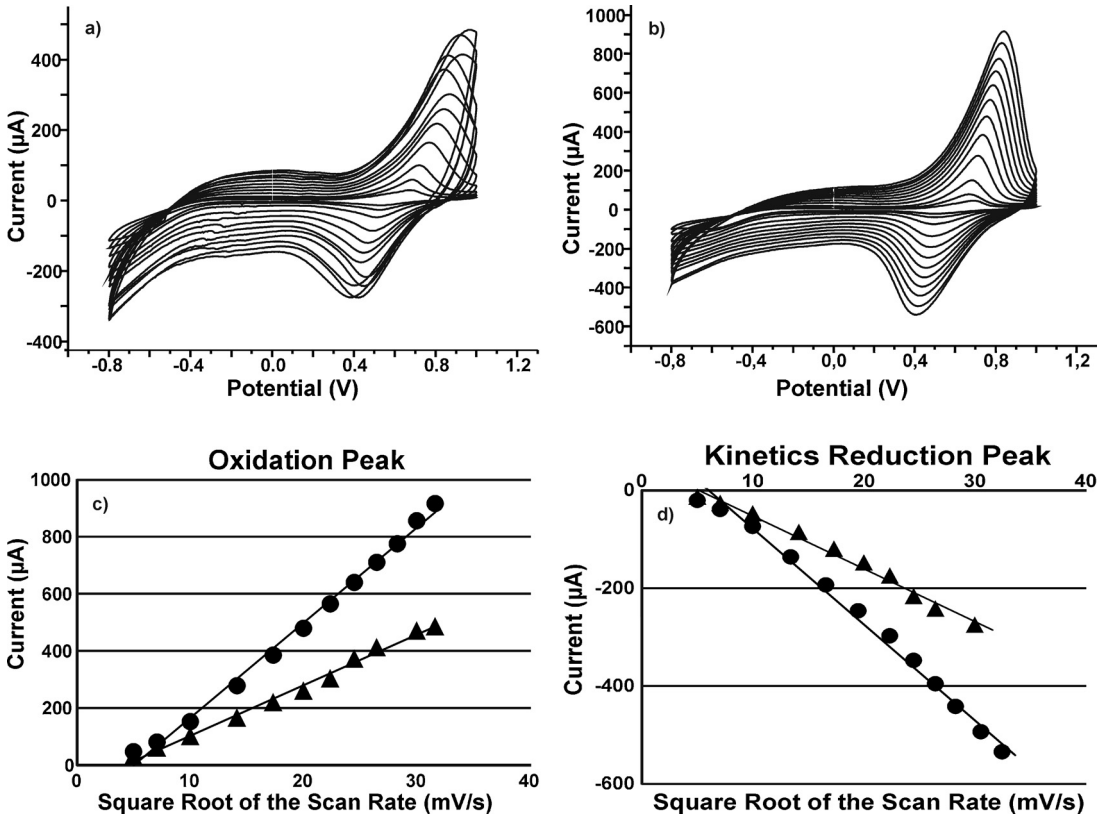

Fig. 7. Top: cyclic voltammograms of (a) LuPc2:DODAB (10:1), (b) LuPc2:DODAB/SAuNPs (10:1/500) registered at scan rates from 10 to 1000 mV s^{-1}; down: (c) plot of I_{pa} vs. $v^{1/2}$ and (d) plot of I_{pc} vs. $v^{1/2}$.

The RRS displays the well-known peaks corresponding to the active vibration modes of the $LuPc_2$ where the bands in the resonance region are clearly enhanced. For this reason, the spectra are dominated by four intense bands at 676 cm^{-1}, 737 cm^{-1}, 775 cm^{-1} and 813 cm^{-1}(associated with the Pc ring), whereas, the bands at higher wavelengths (associated with the pyrrole stretching at 1300–1500 cm^{-1}) are very weak. In contrast, when using the 532 nm laser line, the bands in the 1300–1600 cm^{-1} region associated with the pyrrole are clearly observed [36].

The Raman spectra given in Fig. 6 (top) was obtained point-by-point for a line of 100 μm with step of 1 μm forming a line mapping. These RRS spectra revealed that the films were highly homogeneous with a regular distribution of the phthalocyanine molecules. However, as observed in Fig. 6 (down) the surface-enhanced resonance Raman phenomenon (SERRS) [37] was not clearly observed, and the presence of SAuNP only caused an increase in the fluorescence. The reason of this observation can be attributed to the small size and to the functionalization of the AuNPs. It has been demonstrated that the surface plasmon resonance of small AuNps is dampened when compared to larger particles [34,38]. In addition, the distance dependence of the SERRS effect with the distance nanoparticle–molecule could also be the reason could be the small size of the SAuNP [37].

3.3. Electrochemical characterisation

Cyclic voltammetry of indium tin oxide (ITO) electrodes modified with Langmuir–Blodgett films of $LuPc_2$:DODAB immersed in 0.1 mol L^{-1} KCl (at a scan rate of 0.1 V s^{-1}) showed a quasi-reversible process with the anodic peak at ca. 0.7 V and the cathodic peak at ca. 0.5 V. These peaks were due to the oxidation/reduction of the phthalocyanine ring ($LuPc_2/LuPc_2^+$) and their intensity increased with the proportion of $LuPc_2$ [39]. The insertion of SAuNP reduced the overpotential, causing a shift of the oxidation peak to lower potential values while increasing the intensity. This is illustrated in Fig. 7a and b where the voltammograms obtained from $LuPc_2$:DODAB (10:1) and a $LuPc_2$:DODAB/SAuNPs (10:1/500) at different scan rates (from 10 to 1000 mV s^{-1}) are presented. For instance, at a scan rate of 1000 mV s^{-1}, the peak that appeared at 0.9 V in $LuPc_2$:DODAB moved to 0.77 V in $LuPc_2$:DODAB/SAuNP (10:1/500) while the intensity increased from 460 μA to 920 μA.

In all the LB films studied (using different proportions of $LuPc_2$:DODAB and containing or not SAuNPs), a linear relationship was found between the peak current and the square root of scan rate ($v^{1/2}$) in the range from 10 to 1000 mV s^{-1} indicating a diffusion limited process (Fig. 7c and d). In all cases, regression coefficients were higher than 0.994 for the oxidation peaks and higher than 0.987 for the reduction peaks.

It is worth noting that the curves were steeper for the films containing SAuNPs. For instance, the slope of the curve of the $LuPc_2$:DODAB (1:1) was 10.5, and the slope found in $LuPc_2$:DODAB/SAuNP (1:1/500) was 19.3. This means that the transfer process was two times faster in the presence of SAuNPs. This result proved that the mixed films containing both $LuPc_2$ and SAuNPs showed an excellent dynamic character in the redox process, and also that the charge transfer within the LB film and/or through the electrode interface was facilitated.

The oxidation and reduction of the Pc ring was counterbalanced by the diffusion of ions inside the LB films. Voltammograms carried out in electrolytes with common anions but different cations (i.e. in KCl and $MgCl_2$) were almost identical. In contrast, when changing the anion, important changes were observed. Experiments carried

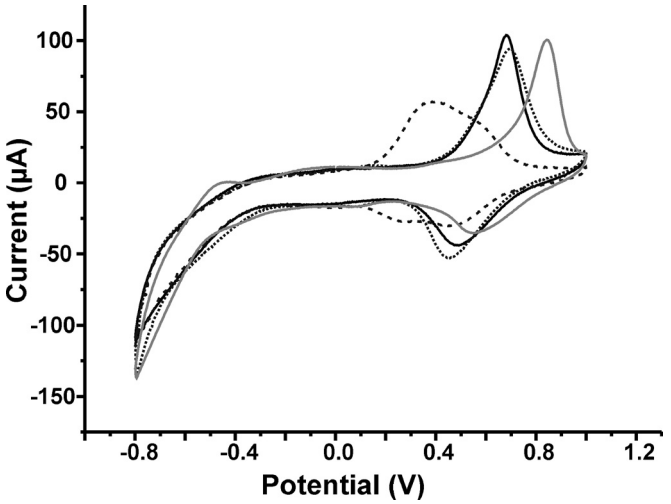

Fig. 8. Cyclic voltammograms of LuPc2:DODAB/SAuNP (1:1/100) immersed in KCl (black line), MgCl2 (dotted line), PBS (grey line) and KClO4 (dashed line).

out in the presence of different electrolytes (Fig. 8) demonstrate that anions (instead of cations) diffused inside the films to maintain the electroneutrality. For this reason, voltammograms obtained in electrolytes containing a common anion were superimposable, whereas voltammograms obtained from solutions differing in the anion were different.

3.4. Electrocatalytic properties

3.4.1. Voltammetric sensors

The electrocatalytic properties of the $LuPc_2$:DODAB and $LuPc_2$:DODAB/SAuNP LB films were tested towards hydroquinone. In order to avoid the polymerisation of the hydroquinone, experiments were carried out in the range from −0.5 to 0.7 V in buffer phosphate (PBS). Under these conditions, the oxidation of the phthalocyanines is no longer observed, and the redox processes registered, correspond to the oxidation/reduction of the hydroquinone. It has to be pointed out that the response registered when using a bare ITO electrode was extremely weak, and the peaks could not be clearly observed. As shown in Fig. 9 (top), LB films of $LuPc_2$:DODAB 10:1 and 1:1 showed electrocatalytic activity for oxidation of hydroquinone, illustrated by a large increase in the intensity of the peaks associated with the oxidation/reduction of the antioxidant and a shift of the anodic peak to lower potentials (that appear at ca. 0.4 V). Films containing low concentrations of the bisphthalocyanine $LuPc_2$:DODAB (1:10) displayed a weak response similar to that observed when using a bare ITO electrode. For this reason, the $LuPc_2$:DODAB (1:10) films were not included in further studies.

Taken into account that the electrocatalytic activity was clearly enhanced by increasing the proportion of $LuPc_2$ in the films, such behaviour can be attributed to the interaction of the hydroquinone with $LuPc_2$ [40].

The presence of SAuNPs was found to increase the electrocatalytic efficiency of the sensors towards oxidation of hydroquinone. This increase was proportional to the concentration of SAuNPs (Fig. 9, down). For instance, the electrocatalytic efficiency of the films was increased by 5% for $LuPc_2$:DODAB/SAuNPs (1:1/100) and 10% for $LuPc_2$:DODAB/SAuNPs (1:1/500) (based on the current intensity of $LuPc_2$:DODAB measured at 0.4 V).

The presence of SAuNPs increased the intensity of the oxidation current by creating active sites and improving the communication within the phthalocyanine films and the electrode. Similar electrocatalytic effects have been observed in electrodes covered with metallic nanoparticles and other organic materials [41,42].

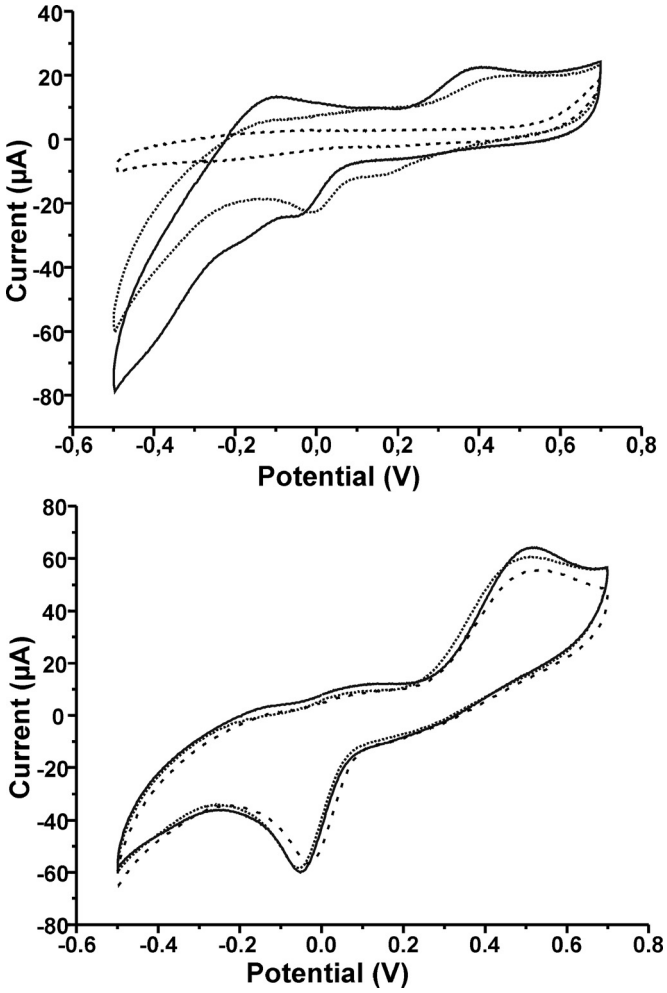

Fig. 9. Up: cyclic voltammograms registered in 40 μmol L^{-1} of hydroquinone using: top: LuPc2:DODAB (10:1) (dotted line); LuPc2:DODAB (1:1) (solid line); LuPc2:DODAB (1:10) (dashed line). Down: LuPc2:DODAB (1:1) (dashed line); LuPc2:

As shown in the previous paragraphs, the peak-to-peak separation and electron transfer kinetics of $LuPc_2$:DODAB/SAuNP modified electrodes changed with the amount of SAuNP inserted in the LB structure. However, it is important to notice that an excess of SAuNP (injecting more than 500 μL of SAuNP under the water subphase) did not produce further improvement leading to a decrease in electrochemical sensitivity and irreproducibility.

The peak current (measured at the voltage of oxidation or reduction of hydroquinone) showed a root square dependence with the scan rate (from 10 to 1000 mV s^{-1}) which indicates diffusion controlled mechanism for the oxidation/reduction of the species in solution. As shown in Table 2 that collects the data corresponding to the anodic waves, the presence of SAuNPs

Table 2
Slope and regression coefficient of the curves obtained by representing the intensity of the anodic peak of the oxidation of hydroquinone (at 0.45 V) vs. the square root of the scan rate (from 10 to 1000 mV s^{-1}).

SAuNPs (μL)	$E = 0.45$V	
	Slope	R^2
$LuPc_2$:DODAB (1:1)	7.3847	0.9987
$LuPc_2$:DODAB/SAuNP (1:1/100)	7.95	0.9988
$LuPc_2$:DODAB/SAuNP (1:1/500)	8.9535	0.9993
$LuPc_2$:DODAB (10:1)	7.4009	0.9979
$LuPc_2$:DODAB/SAuNP (10:1/100)	7.8023	0.9979
$LuPc_2$:DODAB/SAuNP (10:1/500)	8.4641	0.9917

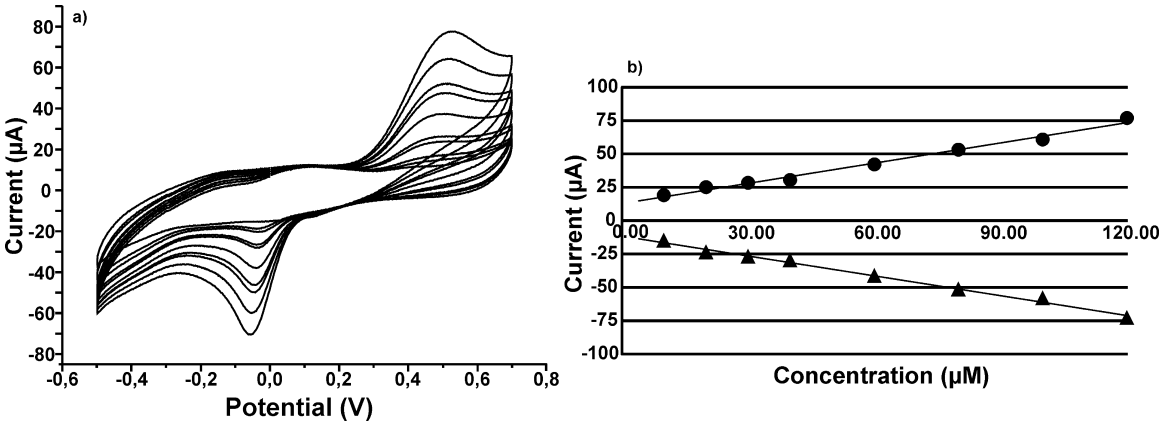

Fig. 10. Response LuPc2:DODAB/SAuNPs 1:1/100 towards hydroquinone (4–150 μmol L^{-1} in PBS).

Table 3
Detection limits calculated for the detection of hydroquinone using LuPc2:DODAB and LuPc2:DODAB/SAuNP nanostructured films.

Sensor	Oxidation				Reduction			
	E (V)	Slope	R^2	LOD (mol L^{-1})	*E* (V)	Slope	R^2	LOD (mol L^{-1})
$LuPc_2$:DODAB (1:1)	0.52	0.4471	0.9888	1.65×10^{-6}	−0.03	−0.4231	0.9889	2.14×10^{-6}
$LuPc_2$:DODAB/SAuNP (1:1/100)	0.52	0.5055	0.9885	9.30×10^{-7}	−0.07	−0.4732	0.9897	5.60×10^{-7}
$LuPc_2$:DODAB/SAuNP (1:1/500)	0.52	0.5254	0.9891	3.30×10^{-7}	−0.08	−0.4872	0.983	4.60×10^{-7}
$LuPc_2$:DODAB (10:1)	0.42	0.5699	0.9923	1.74×10^{-6}	−0.08	−0.4772	0.9938	2.71×10^{-6}
$LuPc_2$:DODAB/SAuNP (10:1/100)	0.48	0.515	0.9984	1.41×10^{-6}	−0.08	−0.3207	0.9949	7.80×10^{-7}
$LuPc_2$:DODAB/SAuNP (10:1/500)	0.6	0.368	0.9914	1.05×10^{-6}	−0.01	−0.2399	0.9892	8.77×10^{-7}

increased the slope of the curve pointing to a favoured charge transfer process. The increase varied between 15% and 22% depending on the sensor.

The intensity of the peaks associated with the phenol increased linearly with the concentration of hydroquinone in the range from 5 μmol L^{-1} to 150 μmol L^{-1} (Fig. 10). The calibration curves were constructed by representing the intensity value of the anodic (ca. 0.45 V) and cathodic (at ca. −0.1 V) waves vs. the hydroquinone concentration. The limits of detection (LOD) were obtained according to the $3s_d\,m^{-1}$ criterion, where *m* is the slope of the calibration curve, and s_d was estimated as the standard deviation (seven repetitions) of the voltammetric signal registered using the blank. The LOD calculated for all the sensors prepared are collected in Table 3. The improvement of the sensitivity caused by the synergistic electrocatalytic effect allowed the $LuPc_2$:DODAB/SAuNP sensors to reach limits of detection in the range of 10^{-6}–10^{-7} mol L^{-1} which are lower than those obtained for the corresponding $LuPc_2$:DODAB electrodes. These results demonstrate that the $LuPc_2$:DODAB/SAuNP nanostructured sensors can be used to quantify the presence of hydroquinone in the range usually present in foods and even below.

The responses were highly reproducible with a coefficient of variation ($n = 10$) lower than 2.0% between similar sensors (same composition). The reproducibility intra-assay was lower than 1.0%.

4. Conclusions

In this article, a method has been developed to prepare nanostructured electrodes of two electrocatalytic materials (functionalised AuNPs and lutetium bisphthalocyanine) using the Langmuir–Blodgett technique.

The surface pressure-mean molecular area isotherms combined with BAM images indicate that SAuNPs are adsorbed into the floating films formed by $LuPc_2$ and DODAB. Spectroscopic and microscopic studies confirm that homogeneous LB films can be transferred to solid substrates.

Electrocatalytic properties of the $LuPc_2$:DODAB/SAuNP electrodes towards the detection of hydroquinone was evidenced by a decrease in the oxidation potential at which oxidation of hydroquinone takes place (peak appears at 0.8 V in bare electrode and at 0.45 V in modified electrodes). It was demonstrated that the SAuNPs and $LuPc_2$ have a synergistic effect in terms of improving electrocatalysis for the detection of hydroquinone as confirmed by the enhancement of the oxidation peak current, (at 0.45 V) and the reduction peak current (at −0.01 V).

Voltammetric responses were proportional to the concentration of hydroquinone between 5 μmol L^{-1} and 150 μmol L^{-1}, and the limit of detection was in the range of 10^{-6}–10^{-7} mol L^{-1} with good reproducibility.

Acknowledgements

Financial support of the CICYT (Grant AGL2012-33535), MEC (Grant PHB2011-0004PC), CAPES/DGU260/12 and Junta de Castilla y León (VA032U13) and PIF-UVa is gratefully acknowledged.

References

[1] G. Bartosz, Food Oxidants and Antioxidants: Chemical, Biological, and Functional Properties, CRC press, Florida, 2013.
[2] O. Makhotina, P.A. Kilmartin, The use of cyclic voltammetry for wine analysis: determination of polyphenols and free sulfur dioxide, Anal. Chim. Acta 668 (2010) 155–165.
[3] R. Prehn, J. Gonzalo-Ruiz, M. Cortina-Puig, Electrochemical detection of polyphenolic compounds in foods and beverages, Curr. Anal. Chem. 8 (2012) 472–484.
[4] D. Narducci, There's plenty of room inside, Sci. Adv. Mater. 3 (2011) 426–435.
[5] A.C. Chen, S. Chatterjee, Nanomaterials based electrochemical sensors for biomedical applications, Chem. Soc. Rev. 42 (2013) 5425–5438.
[6] F.W. Campbell, R.G. Compton, The use of nanoparticles in electroanalysis: an updated review, Anal. Bioanal. Chem. 396 (2010) 241–259.
[7] Y.G. Zhou, F.W. Campbell, S.R. Belding, R.G. Compton, Nanoparticle modified electrodes: surface coverage effects in voltammetry showing the transition from convergent to linear diffusion. The reduction of aqueous chromium(III) at silver nanoparticle modified electrodes, Chem. Phys. Lett. 497 (2010) 200–204.

[8] F. Pena-Pereira, R.M.B.O. Duarte, A.C. Duarte, Immobilization strategies and analytical applications for metallic and metal-oxide nanomaterials on surfaces, Trends Anal. Chem. 40 (2012) 90–105.
[9] X. Shan, I. Díez-Pérez, L. Wang, P. Wiktor, Y. Gu, L. Zhang, W. Wang, J. Lu, S. Wang, Q. Gong, J. Li, N. Tao, Imaging the electrocatalytic activity of single nanoparticles, Nat. Nanotech. 7 (2012) 668–672.
[10] J. Jiang, Functional Phthalocyanine Molecular Materials Series: Structure and Bonding, 13, Springer, Berlin, 2010.
[11] M.L. Rodriguez-Mendez, Sensing properties of phthalocyanines, in: C.S. Grimes, E.C. Dickey, M.V. Pishko (Eds.), Encyclopedia of Sensors, vol. 9, America Scientific Publishers, California, 2006, pp. 111–134.
[12] J.H. Zagal, S. Griveau, J.F. Silva, T. Nyokong, F. Bedoui, Metallophthalocyanine-based molecular materials as catalysts for electrochemical reactions, Coord. Chem. Rev. 254 (2010) 2755–2794.
[13] M. Bouvet, P. Gaudillat, J.M. Suisse, Phthalocyanine-based hybrid materials for chemosensing, J. Porphyr. Phthalocyanines 17 (2013) 913–919.
[14] A.B. Sorokin, E.V. Kudrik, Phthalocyanine metal complexes: versatile catalysts for selective oxidation and bleaching, Catal. Today 159 (2011) 37–46.
[15] L. Valli, Phthalocyanine-based Langmuir–Blodgett films as chemical sensors, Adv. Colloid Interface Sci. 116 (2005) 13–44.
[16] M.L. Rodriguez-Mendez, M. Gay, J.A. de Saja, New insights into sensors based on radical bisphthalocyanines, J. Porphyr. Phthalocyanines 13 (2009) 1159–1167.
[17] D. Volpati, P. Alessio, A.A. Zanfolim, F.C. Storti, A.E. Job, M. Ferreira, A. Riul, O.N. Oliveira Jr., C.J.L. Constantino, Exploiting distinct molecular architectures of ultrathin films made with iron phthalocyanine for sensing, J. Phys. Chem. B 112 (2008) 15275–15282.
[18] F.J. Pavinatto, E.G.R. Fernandez, P. Alessio, C.J. Constantino, J.A. de Saja, V. Zucollotto, O.N. Oliveira Jr., C. Apetrei, M.L. Rodriguez-Mendez, Optimized architecture for tyrosinase-containing Langmuir–Blodgett films to detect pyrogallol, J. Mater. Chem. 21 (2010) 4995–5003.
[19] T. Nyokong, E. Antunes, Influencece of nanoparticle materials on the photophysical behavior of phthalocyanines, Coord. Chem. Rev. 257 (2013) 2401–2418.
[20] V.P. Chauke, W. Chidawanyika, T. Nyokong, The electrochemical behaviour of gold nanoparticle–tantalum (V) phthalocyanine composites: applications towards the electroanalysis of bisphenol A, Electroanalysis 23 (2011) 487–496.
[21] C. Hone, P.I. Walker, R. Evans-Gowing, S. Fitzgerald, A. Beeby, I. Chambrier, M.J. Cook, D.A. Russell, Generation of cytotoxic singlet oxygen via phthalocyanine-stabilized gold nanoparticles: a potential delivery vehicle for photodynamic therapy, Langmuir 18 (2002) 2985–2987.
[22] M. Pal, V. Ganesan, Zinc phthalocyanine and silver/gold nanoparticles incorporated MCM-41 type materials as electrode modifiers, Langmuir 25 (2009) 13264–13272.
[23] W.S. Alencar, F.N. Crespilho, M.V.A. Martins, V. Zucolotto, O.N. Oliveira Jr., W.C. Silva, Synergistic interaction between gold nanoparticles and nickel phthalocyanine in layer-by-layer (LbL) films: evidence of constitutional dynamic chemistry (CDC), Phys. Chem. Chem. Phys. 11 (2009) 5086–5091.
[24] P.H.B. Aoki, P. Alessio, J.A. de Saja, C.J.L. Constantino, Incorporation of Ag nanoparticles into membrane mimetic systems composed by phospholipid layer-by-layer (LbL) films to achieve surface-enhanced Raman scattering as a tool in drug interaction studies, J. Raman Spectrosc. 41 (2010) 40–48.
[25] K.D. Comeau, M.V. Meli, Effect of alkanethiol chain length on gold nanoparticle monolayers at the air–water interface, Langmuir 28 (2012) 377–381.
[26] P.J. Deisinger, T.S. Hill, J.C. English, Human exposure to naturally occurring hydroquinone, J. Toxicol. Environ. Health 47 (1996) 31–46.
[27] M. Linaje, M.C. Quintanilla, A. Gonzalez, J.L. Valle, G. Alcaide, M.L. Rodriguez-Mendez, Improvement of the synthesis of lutetium bisphthalocyanine using the Taguchi method, Analyst 125 (2000) 341–346.
[28] R.E. Clavijo, D. Battisti, R. Aroca, G.J. Kovacs, C.A. Jennings, Surface-enhanced Raman-spectra and gas chemisorption of Langmuir–Blodgett layers of lutetium and ytterbium, Langmuir 8 (1992) 113–117.
[29] M. Maitrot, G. Guillaud, B. Boudjema, J.J. Andre, H. Strzelecka, J. Simon, R. Even, Lutetium bisphthalocyanine: the 1st molecular semiconductor. Conduction properties of thin-films of p-doped and n-doped materials, Chem. Phys. Lett. 133 (1987) 59–62.
[30] J. Souto, L. Tomilova, R. Aroca, J.A. de Saja, Spectroscopic studies of Langmuir–Blodgett monolayers of praseodymium bisphthalocyanines, Langmuir 8 (1992) 942–946.
[31] M.I. Viseu, A.M. Gonçalves da Silva, P. Antunes, S.M.B. Costa, Organization of cationic porphyrins in mixed Langmuir–Blodgett films. An absorption and steady-state fluorescence study, Langmuir. 18 (2002) 5772–5781.
[32] M.T. Martin, D. Möbius, Enhanced binding of porphyrin by a laterally organized monolayer, Thin Solid Films 284–285 (1996) 663–666.
[33] M.L. Rodriguez-Mendez, Y. Gorbunova, J.A. de Saja, Spectroscopic properties of Langmuir–Blodgett films of lanthanide bis(phthalocyanine)s exposed to volatile organic compounds. Sensing applications, Langmuir 18 (2002) 9560–9565.
[34] X. Huang, M.A. El-Sayed, Optical properties and implementations in cancer diagnosis and photothermal therapy, J. Adv. Res. 1 (2010) 13–28.
[35] M. Moskovits, Surface-enhanced Raman spectroscopy: a brief retrospective, J. Raman Spectrosc. 36 (2005) 485–496.
[36] M.L. Rodriguez-Mendez, R. Aroca, Spectroscopic and electrochemical properties of thin solid films of yttrium bisphthalocyanine, Spectrochim. Acta A 49 (1993) 965–973.
[37] R. Aroca, N. Pieczonka, A.P. Kam, Surface-enhanced Raman scattering and SERRS imaging of phthalocyanine mixed films, J. Porphyr. Phthalocyanines 5 (2001) 25–32.
[38] E.C. Le Ru, P.G. Etchegoin, M. Meyer, Enhancement factor distribution around a single surface-enhanced Raman scattering hot spot and its relation to single molecule detection, J. Chem. Phys. 125 (2006) 204701.
[39] E.G.R. Fernandes, L.C. Brazaca, M.L. Rodriguez-Mendez, J.A. de Saja, V. Zucolotto, Immobilization of lutetium bisphthalocyanine in nanostructured biomimetic sensors using the LbL technique for phenol detection, Biosens. Bioelectron. 26 (2011) 4715–4719.
[40] M. Gay Martin, M.L. Rodriguez-Mendez, J.A. de Saja, Films of lutetium bisphthalocyanine nanowires as electrochemical sensors, Langmuir 26 (2010) 19217–19224.
[41] U.P. Azad, V. Ganesan, Influence of metal nanoparticles on the electrocatalytic oxidation of glucose by poly(Ni(Pi)teta) modified electrodes, Electroanalysis 22 (2010) 575–583.
[42] M. Pal, V. Ganesan, Zinc phthalocyanine and silver/gold nanoparticles incorporated MCM-41 type materials as electrode modifiers, Langmuir 25 (2009) 13264–13272.